Proc. Natl. Acad. Sci. USA
Vol. 92, pp. 9279–9283, September 1995
Biophysics

Nuclear magnetic dipole interactions in field-oriented proteins: Information for structure determination in solution

(myoglobin/NMR/paramagnetic proteins)

J. R. TOLMAN*, J. M. FLANAGAN†, M. A. KENNEDY‡, AND J. H. PRESTEGARD*

*Department of Chemistry, Yale University, New Haven, CT 06520-8107; †Biology Department, Brookhaven National Laboratories, Upton, NY 11937; and ‡Environmental and Molecular Sciences, Battelle Northwest Laboratory, Richland, WA 99352

Communicated by Frederic M. Richards, Yale University, New Haven, CT, July 3, 1995

ABSTRACT **The measurement of dipolar contributions to the splitting of ^{15}N resonances of ^{1}H–^{15}N amide pairs in multidimensional high-field NMR spectra of field-oriented cyanometmyoglobin is reported. The splittings appear as small field-dependent perturbations of normal scalar couplings. Assignment of more than 90 resonances to specific sequential sites in the protein allows correlation of the dipolar contributions with predictions based on the known susceptibility and known structure of the protein. Implications as an additional source of information for protein structure determination in solution are discussed.**

Within the past 15 years, NMR has emerged as a powerful approach to the study of protein structure in solution (1, 2). The approach relies on distance constraints extracted from nuclear Overhauser effects (NOEs) and typically proceeds in three stages: assignment of backbone resonances to specific sequential sites, identification of secondary structure elements, and determination of a tertiary fold. The latter stage is particularly demanding because it requires that a large number of long-range distance constraints be extracted from NOE data and assigned to specific proton pairs. Because NOEs drop off with the inverse 6th power of the internuclear distance, the pairs tend to arise from direct side-chain–side-chain contacts, contacts involving protons which are among the most difficult to assign. Opportunities to supplement long-range distance constraints with other types of structural data would, therefore, be welcome.

We demonstrate here that NMR spectra of certain proteins, taken at very high field, may contain data that can usefully complement NOEs in determining a tertiary fold. The data come from residual dipolar contributions to the scalar couplings normally seen in high-resolution spectra. These appear when the protein has a slightly preferred orientation in a magnetic field. The contributions are angle dependent and can yield constraints for the orientation of one structural element relative to another structural element. In our case, we use a 17.5-kDa protein, cyanometmyoglobin, which has a very highly anisotropic paramagnetic susceptibility to achieve preferred orientation. Myoglobin crystals have been previously shown to orient in a magnetic field because of their anisotropy (3). Bothner-By and co-workers (4) also showed years ago that orientational effects on NMR spectra of single molecules in solution could be observed if fields and resolution were high enough. That these effects can be observed in an isolated protein molecule, and that the effects can provide useful structural constraints, has awaited higher fields (17.5 T) and multidimensional NMR experiments for the detection and assignment of ^{15}N resonances in an isotopically labeled protein.

Theory. The dipolar interaction between two spin 1/2 nuclei in the high-field limit is given by the formula

$$H_D = -[\gamma_i\gamma_j h/(2\pi^2 r^3)]\langle(3\cos^2\theta - 1)/2\rangle I_{zi}I_{zj}, \quad [1]$$

where the γ values are the gyromagnetic ratios for the nuclei, h is Plank's constant, r is the distance between the nuclei, θ is the angle between the internuclear vector and the applied magnetic field, and the I_z values are spin operators for the two nuclei (5). In principle, the interaction would manifest itself as a splitting of NMR resonances into doublets. When nuclear pairs are directly bonded, as in a ^{1}H–^{15}N amide pair, for example, the interaction would add to the scalar coupling normally seen in nondecoupled high-resolution NMR spectra.

Variations in scalar couplings due to dipolar effects are not normally observed in high-resolution spectra. This is because of motional averaging denoted by the brackets in Eq. **1**. All motions occurring on time scales short compared the reciprocal of the dipolar interaction in Hz ($<10^{-3}$ s for ^{1}H–^{15}N and $r = 1$ Å) contribute to the averaging, including molecular tumbling in solution. For diamagnetic molecules at moderate field strengths, molecules have little preference in orientation, the tumbling samples a nearly isotropic distribution, and the term inside the bracket goes to zero. If, however, a molecule has a preference in orientation, an average interaction would persist, and the splittings of resonances would vary from their nominal scalar couplings by an amount that depends on the angle θ.

Actually, most molecules have preferred orientations in the presence of a magnetic field, because most have anisotropic magnetic susceptibility tensors, χ (6). Different orientations result in induced magnetic moments of different sizes and the energies of interaction of these moments with the magnetic field are different. An expression for the distribution function that results from sampling with a Boltzmann distribution in a low-energy limit is given as

$$P(\theta',\phi) = (N)^{-1}\{1 + B^2(4\,\mathrm{kT})^{-1}[\Delta\chi_a(2/3)(3\cos^2\theta' - 1) + \Delta\chi_r(\sin^2\theta'\cos 2\phi)]\}, \quad [2]$$

where B is the applied magnetic field, $\Delta\chi_a$ and $\Delta\chi_r$, respectively, are the axial and rhombic anisotropies of the susceptibility tensor, θ' and ϕ describe the orientation of the susceptibility tensor relative to the magnetic field, and N is a normalization constant. Under many circumstances, the departure of $P(\theta',\phi)$ from $(N)^{-1}$ (an isotropic distribution) is insignificant, showing consistency with most observations in solution. Conditions where departures are significant and residual interactions are observable include those where the anisotropy of χ is large and the applied fields B are large.

It is clear in Eq. **1** that measurement of residual couplings can provide powerful structural constraints through their relationship to the angle θ and the internuclear distance r. The effects of averaging simply need to be separated. When many

The publication costs of this article were defrayed in part by page charge payment. This article must therefore be hereby marked "*advertisement*" in accordance with 18 U.S.C. §1734 solely to indicate this fact.

Abbreviations: NOE(SY), nuclear Overhauser effect (spectroscopy); HSQC, heteronuclear single quantum coherence.

interactions exist within the same molecule, and they are averaged by the same motion, this separation is possible. The conditions for structural application are therefore well defined: large anisotropy of susceptibility, high magnetic field, and numerous interactions, preferably ones where either r or θ is known.

Molecular System. Myoglobin does have a highly anisotropic susceptibility, and any protein has a large number of potential dipolar interactions, but the choice of a protein, and myoglobin in particular, deserves some further discussion. It is primarily the ability to produce ^{15}N-enriched forms of proteins by molecular biological techniques and the ability to study these molecules by multidimensional NMR methods that make proteins a good choice for study. ^{15}N enrichment leads to directly bonded ^{1}H and ^{15}N pairs in all amide bonds. These pairs have substantial dipolar interactions, are well distributed over the molecule, and have an internuclear distance, r, that is reasonably invariant. The resonances arising from these pairs are assignable to specific sequential sites using the variety of multidimensional NMR methods that have evolved over the past several years (1), and couplings are easily resolvable in the indirectly detected ^{15}N dimension of many of these experiments.

Myoglobin in particular is a good choice for several reasons. Horrocks *et al.* (7) have calculated the paramagnetic susceptibility tensor for cyanometmyoglobin and Emerson and La Mar (8) have oriented it in the protein. Using this work, and assuming the paramagnetic component of the susceptibility will dominate the anisotropy, we predict that there should be residual dipolar couplings of -3 to $+4.5$ Hz for ^{1}H–^{15}N amide pairs at 17.5 T and 303 K. The electron spin in cyanometmyoglobin also relaxes rapidly, making high-resolution NMR experiments possible (9). Several groups have now shown that high-resolution NMR experiments, including multidimensional experiments normally used for resonance assignment, are applicable to certain paramagnetic proteins (10, 11). In the case of myoglobin, the recent publication of a complete set of assignments for ^{1}H and ^{15}N resonances in the diamagnetic carboxy form also may aid assignment by allowing the correlation of chemical shifts and NOE connectivity patterns in the diamagnetic versus paramagnetic states (12).

MATERIALS AND METHODS

Expression and Growth of Myoglobin. Myoglobin was expressed in *Escherichia coli* BL26(DE3) directed from the plasmid pET13MB, which was developed for production of deuterated myoglobin for neutron diffraction studies (14). Production of ^{15}N-labeled myoglobin was accomplished in Mops minimal medium containing $^{15}NH_4Cl$ (99% enrichment; Cambridge Isotope Laboratories, Cambridge, MA) as the sole nitrogen source (13). The myoglobin-producing cells were grown at 37°C to an OD_{600} of 1.0, at which point the temperature was lowered to ≈23°C and protein production was induced by addition of isopropyl β-D-thiogalactopyranoside to a final concentration of 0.4 mM. The culture was grown an additional 20 h ($OD_{600} \approx 4.0$), after which time the cells were harvested by low-speed centrifugation. Cell pellets were frozen and stored at −70°C until they were used.

Separation of Myoglobin. Myoglobin was separated according to the procedure described by F. Shu (14). Briefly, 6–10 g of *E. coli* BL26(DE3)-pET13MB paste was thawed by suspension in 50 ml of 50 mM Tris·HCl, pH 8.0/25% (wt/vol) sucrose/5 mM EDTA/1 mM dithiothreitol (DTT)/0.05 mM phenylmethylsulfonyl fluoride. DNase I (1 mg) and hen egg white lysozyme (50 mg) were added and the suspension was incubated for 30 min on ice. At the end of this period, deoxycholate was added to a final concentration of 0.08% followed by incubation for an additional 15 min. To promote hydrolysis of the DNA, $MgCl_2$ and $MnCl_2$ were added to final concentrations of 10 and 1 mM, respectively. After a 30-min incubation, the majority of the 260-nm-absorbing material was precipitated by dropwise addition of 10% polyethylenimine to a final concentration of 0.25%, and the precipitate was removed by centrifugation at 12,000 × g for 30 min. Normally, a second extraction of the pellet with lysis buffer was required to recover all of the myoglobin.

***In Vitro* Heme Reconstitution of Myoglobin.** A 2-fold molar excess of solid hemin (Aldrich) was dissolved in a minimum volume of 0.1 M NaOH and reconstitution was carried out at 4°C by dropwise addition to the slowly stirred lysate. The degree of reconstitution was followed by examining the ratio of the absorbance at 280 nm to that at 410 nm throughout the reconstitution procedure. At this stage, a ratio of 1.5 was taken as an indication that the myoglobin was fully reconstituted. The reconstitution reaction mixture was allowed to sit on ice for an additional 1 h. Excess solid hemin and any precipitate were then removed by centrifugation at 12,000 × g for 30 min.

Myoglobin Purification Procedure. The pH of the deep red supernatant was carefully adjusted to pH 6.0 by addition of concentrated acetic acid and then loaded onto a 50-ml SP cation-exchange column [Fractogel EMD SP-650(M); EM Science] equilibrated with 50 mM Mes, pH 6.0/1 mM DTT. The column was washed with 100 ml of this buffer and the bound proteins were eluted in a 500-ml linear 0–0.4 M NaCl gradient. The peak fractions were pooled and concentrated to ≈2 ml. The concentrated myoglobin was further purified by size-exclusion chromatography on a TSK-250 column (600 × 21.5 mm) (Bio-Rad) equilibrated with 25 mM Mes, pH 6.0/100 mM NaCl.

Preparation of NMR Samples. The pooled fractions from the size-exclusion column were exchanged into 90% H_2O/10% $^{2}H_2O$, which was 200 mM NaCl and 25 mM KCN. The pH was adjusted to 8.6 by addition of solutions of HCl or NaOH, and the sample, ≈5 mM myoglobin, was divided between two identical 5-mm NMR tubes (Shigemi, Tokyo). The pH is typical of what has been used for analysis of nonexchangeable proton spectra of cyanometmyoglobin in the past (8), but it is high for analysis of exchangeable protons such as amide protons. We nevertheless maintained this pH because of concern for the stability of the cyanide complex. We have subsequently discovered that these concerns are unfounded (9). The oxidation state and degree of proper heme insertion were verified by observation and integration of hyperfine shifted resonances from the heme group (9). We found that the sample was fully oxidized but only ≈60% of the heme was in the proper orientation. Addition of cyanide effectively stops equilibration of heme orientation in the myoglobin binding site and cyanide was apparently added too early. Despite these minor problems, excellent spectra could be acquired.

NMR Spectroscopy. Proton-detected heteronuclear NMR experiments were collected on three different spectrometers—a GE Omega PSG operating at 500 MHz, a Varian Unity Plus operating at 600 MHz, and a Varian Unity Plus operating at 750 MHz. A three-dimensional NOE heteronuclear single quantum correlation spectrum (NOESY-HSQC) was collected at 600 MHz for the purpose of spectral assignment. The pulse sequence uses gradient-enhanced water-flipback strategies introduced by Grzesiek and Bax (15). These sequences are important for operation at high pH, where exchange of amide protons with water protons is fast. Over a total acquisition period of 52 h, 64 complex t_1 points, 128 complex t_2 points, and 512 complex t_3 points were collected at an average recycling rate of 0.7 s^{-1} using sweep widths of 1800, 7500, and 9000 Hz, respectively. A NOE mixing time of 50 ms was chosen to provide a reasonable blend of interresidue and intraresidue connectivities.

A specially designed two-dimensional HSQC experiment was used to collect data at 750 MHz from which splittings of the ^{15}N resonance in the indirect dimension could be measured

(coupling-enhanced HSQC) (J.R.T. and J.H.P., unpublished data). The sequence is based on a gradient-enhanced water-flipback HSQC (16) but incorporates an extra ^{15}N 180° pulse during t_1 evolution. The pulse was simultaneous with the usual 180° ^1H pulse, but both were positioned accordion style to allow pure dipolar splitting evolution for half the period and chemical shift plus dipolar splitting evolution for the other half the period. This sequence scaled chemical shift dispersion so that a smaller spectral width and longer evolution time could be used. For the 750-MHz data set, 200 complex t_1 points were collected with a total t_1 acquisition time of 182 ms. The total experiment time was 14 h, with a recycling rate of 0.5 s^{-1}. For the 500-MHz coupled HSQC data, where chemical shift resolution proved to be a major concern, a standard gradient-enhanced water-flipback HSQC experiment modified to allow coupling evolution during t_1 was acquired. The total experimental duration was 17 h, with a recycle rate of 0.5 s^{-1}; 300 complex t_1 points were acquired for a t_1 acquisition time of 210 ms.

Data Processing. FELIX 3.1 software (Biosym Technologies, San Diego) was used to process all of the acquired NMR data. For the three-dimensional NOESY-HSQC data set, the data were zero-filled in order to produce a final data matrix, which was 512 × 512 × 128 points. In the D1 (^{15}N) dimension, the size of the data was extended by 33% via linear prediction. Sinebell window functions, shifted 60°, 30°, and 90° in the three dimensions, respectively, were applied prior to Fourier transformation. The two-dimensional HSQC data sets were zero-filled in order to produce $2K \times 2K$ data matrices. A sinebell window function, which was shifted by 70° and which had a skew factor of 0.7, was applied in the D2 dimension. In D1, an unshifted sinebell was applied prior to Fourier transformation in order to enhance resolution. The software package PIPP, provided by Dan Garrett (National Institutes of Health), was used to find peak centers in both the coupled HSQC 500-MHz data set and the coupling enhanced HSQC 750-MHz data set. From these tabulated peak centers, the measured ^{15}N splittings could readily be computed.

RESULTS

Normally, assignment of resonances to specific sequential sites in a molecule of unknown structure would have to proceed by the sequential assignment strategies based on the initial work of Wüthrich and co-workers (17). For myoglobin, the structure is known (18) and assignments for the diamagnetic carboxy form of the protein at pH 5.6 and 35°C are available (12). We can, therefore, approach assignment in a slightly different way. Myoglobin is a predominantly α-helical protein from which one would expect a very characteristic pattern of interresidue NOE connectivities; namely strong amide (i) to amide ($i \pm 1$), and moderate amide (i) to α ($i - 1$) connectivities. These patterns allow identification of strings of sequential residues. We would also expect major chemical shift differences between corresponding resonances in the carboxy and cyanomet forms to be due to pseudocontact shifts. The expected shift differences can be calculated based on the susceptibility tensor orientation work of Emerson and La Mar (8) and options for assignment restricted to those consistent with the work of Thériault *et al.* (12). Based on these expectations, we were able to sequentially assign ^1H–^{15}N pairs by just a single three-dimensional NOESY-HSQC experiment.

Fig. 1 shows columns emanating from specific intraresidue ^1H–^{15}N cross peaks in this three-dimensional spectrum. A region that turns out to encompass helix A has been chosen for illustration. Lines show the expected amide–amide and amide–α connectivities. In many cases, additional intraresidue and interresidue amide β connectivities aid in residue type assignment. In Table 1 the pseudocontact shift information supporting assignment is shown—namely, the observed and

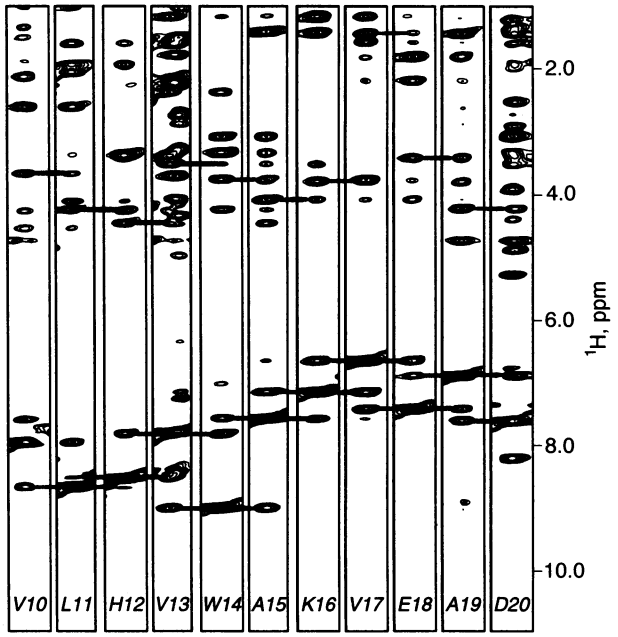

FIG. 1. Strip plots taken at sequential amide ^1H–amide ^{15}N chemical shifts from a three-dimensional NOESY-HSQC spectrum of cyanometmyoglobin. Strips shown correspond to most of helix A. Lines indicate amide–amide NOE connectivities.

predicted shifts for the amide protons and amide nitrogens. A region from helix E, where pseudocontact contributions are large, is shown for illustration. The agreement is excellent in spite of the rather large difference in pH between our work and the carboxy work by Thériault *et al.* (12).

In all, ≈90 amide pairs have been assigned. Additional assignments are summarized on the coupling-enhanced 750-MHz HSQC spectrum in Fig. 2. Note that there are two peaks on a column for each amide site. While most variations are small compared to the typical ^{15}N line width, they are measurably different. Splittings range from 96 to 90 Hz. If scalar couplings alone were responsible for the splitting, nearly all pairs would be split by 94 ± 1 Hz.

The splittings are also field dependent; according to Eq. **2**, the dipolar contributions should increase by a factor of 2.25 in going from 500 to 750 MHz. This field dependence can be exploited to allow separation of the scalar and dipolar contributions to the observed splitting. Variations are again small; however, they are observable. Fig. 3 shows superimposed columns for W14 and for G25. Spectra with dotted and solid lines are taken from the 750- and 500-MHz spectra, respec-

Table 1. Comparison of observed shifts and shifts calculated using pseudocontact corrections

	Chemical shift				Pseudocontact shift	
	Calculated		Observed		Calculated	
Residue	^{15}N	^1H	^{15}N	^1H	^{15}N	^1H
G65	107.9	9.65	106.8	9.22	1.79	1.59
V66	120.8	7.88	119.6	7.50	0.44	0.56
T67	122.6	7.78	122.5	7.34	−0.55	−0.11
V68	119.1	6.99	120.1	6.71	−2.11	−0.67
L69	115.4	7.38	115.8	7.35	−0.96	−0.53
T70	116.7	7.73	116.9	7.78	−0.96	−1.06
A71	123.3	5.95	123.4	6.07	−1.48	−1.83
L72	116.8	7.19	117.0	7.10	−1.27	−1.49
G73	107.0	8.28	107.1	8.35	−0.61	−0.74
A74	121.0	7.01	121.0	7.10	−0.43	−0.55

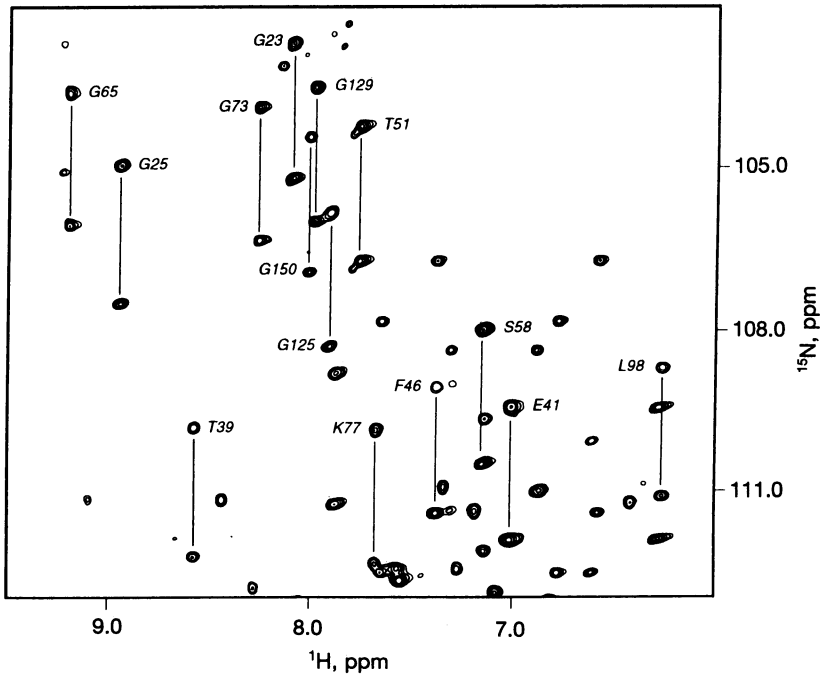

FIG. 2. Expanded region of a coupling-enhanced HSQC spectrum acquired at 750 MHz. Assigned doublets are indicated with a vertical line.

tively. In the case of G25, the splitting increases slightly with field, indicating a negative contribution from dipolar coupling (the scalar coupling is negative), and in the case of W14 the splitting decreases with field, indicating a positive dipolar coupling.

A better demonstration of the existence of dipolar contributions can be obtained by using the known structure and susceptibility of myoglobin to calculate dipolar contributions (Eqs. **1** and **2**) and comparing these to dipolar contributions extracted from the observed field dependence of splittings. Splittings can also be extracted more accurately by fitting peaks in two-dimensional data sets than by visually comparing peaks in a single column. The correlation of observed splittings with calculated splittings is displayed in Fig. 4. Only data from 37 doublets that have a high signal/noise ratio and are well resolved at both 750 and 500 MHz are included. The extracted dipolar contributions are plotted on the abscissa, and the predicted dipolar contributions are plotted on the ordinate. The correlation coefficient for the best-fit line is 0.7, the slope is 1.1, and the intercept is −1.2.

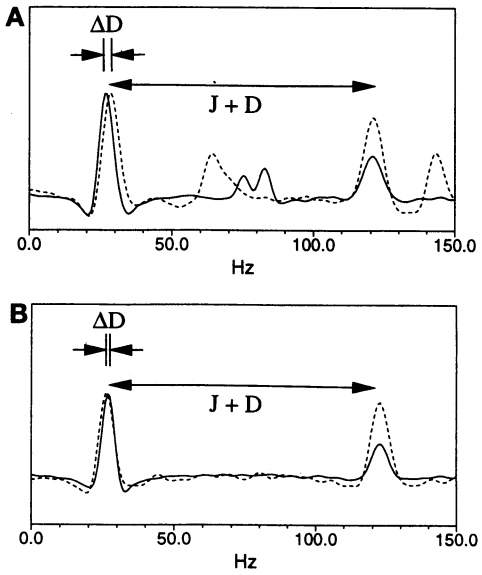

FIG. 3. Superimposed slices taken at the same ^{1}H chemical shift from 500 MHz (solid line) and 750 MHz (dotted line) HSQC data sets. (*A*) Superposition of slices taken through the doublet assigned to W14. Measured difference in splitting, ΔD, is approximately −1.5 Hz. (*B*) Superposition of slices taken through the doublet assigned to G25. Measured difference in splitting, ΔD, is approximately +0.5 Hz.

DISCUSSION

From the above results it is clear that dipolar contributions to the splittings of ^{1}H–^{15}N pairs in myoglobin are observable. The correlation demonstrated in Fig. 4 is actually quite good given the possible sources of error. There will, of course, be some error associated with our precision of measurement (±1.0 Hz). Our assumption that all N–H bond lengths are 1.0 Å is not

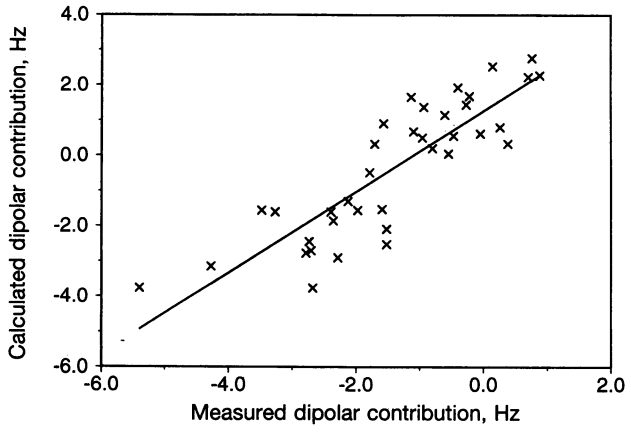

FIG. 4. Measured dipolar contribution to ^{15}N–^{1}H splittings at 750 MHz plotted against theoretical contributions at 750 MHz calculated from the neutron structure and using Eqs. **1** and **2**. *J* has been separated from *D* by using the expected theoretical field dependence of *D* and the splittings were measured at both 500 and 750 MHz. Line indicates resulting least-squares fit of the data. Correlation coefficient is 0.70. Note that we consider measured splittings to be positive even though the scalar ^{15}N–^{1}H one bond coupling is negative.

strictly accurate. The angles of N–H vectors taken from the neutron diffraction structure will have some imprecision. And the assumption that the anisotropy of the paramagnetic susceptibility accurately represents that of the total susceptibility may be wrong. The marginally significant nonzero intercept may also suggest some uniform field-dependent contribution to splittings for which there is currently no theoretical basis. Despite these possibilities, the data in Fig. 4 clearly show that the direction and magnitude of the splittings are consistent with analysis using Eqs. **1** and **2** and the structure of myoglobin as determined from neutron diffraction (18).

Given the observability of dipolar contributions and demonstrated utility of Eqs. **1** and **2**, a more important question is, If the structure of myoglobin were not known, could measured dipolar splittings provide primary information needed to build a structural model? In these cases, assignment strategies would have to be a little different from that presented above. Calculation of pseudocontact shifts would not be an option, and very likely an experiment based on through-bond connectivities would be needed to complete sequential assignments. But once this was done we would know secondary structure based on the NOE data; for an α-helical protein we would know how the sequence divided up into more or less rigid α-helical segments. At this point, we believe that dipolar constraints could replace some of the long-range NOE data that are so essential for determining a tertiary fold. For example, using Eqs. **1** and **2** to interpret the data presented in Figs. 3 and 4, we know that the N–H vector for residue 14 must be directed nearly along the principal axis of the susceptibility tensor, because its dipolar coupling contribution to the observed splitting is near the negative extreme of the distribution. We also know that the N–H vector for residue 25 must be at an angle of nearly 90° relative to the same axis, because its dipolar coupling contribution to the observed splitting is near the positive extreme of the distribution. These residues are parts of helix A and helix B, respectively. Since N–H vectors are more or less parallel to helix axes, their direction should approximately reflect the orientation of the helices in which they are found. Although the splitting measured for G25 provided our only constraint for the B helix, the predicted orientation of helix A was reinforced by measured splittings for four additional assigned N–H pairs. Fig. 5 depicts helices A and B as they occur in the neutron diffraction structure. The orientations, in fact, agree with our predictions.

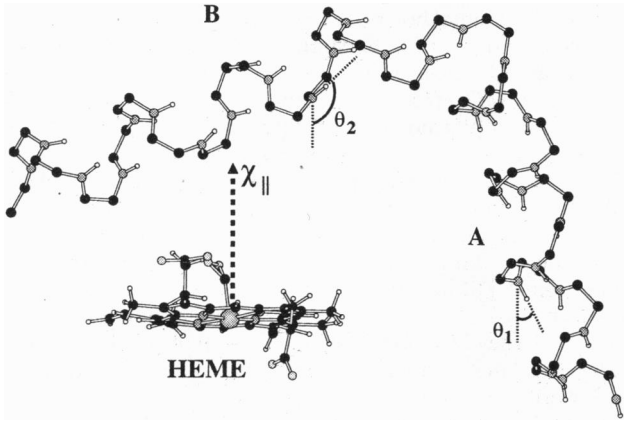

FIG. 5. Helices A and B along with the heme group taken from the neutron structure of carboxymyoglobin (18). Principal axis of the paramagnetic susceptibility tensor has been indicated with θ_1 and θ_2 denoting the angles subtended by this principal axis and selected amide internuclear vectors from helices A and B, respectively.

For other helices, the situation is more complex because the inverse of the angular function in Eq. **1** is multivalued and the axial term in Eq. **2** does not always dominate. However, systematic representation of constraints based on these equations should be possible, and when combined with short-range NOE constraints, and covalent constraints from the primary structure, a more general structure determination protocol should result. Measurements with the precision presented above will clearly be useful in applying this protocol, not so much because they are accurate, but because a very large number of measurements can be made. Also, it is important to realize that the size of the effect, and in some cases the precision of measurement, will increase with field squared. NMR instruments operating at 17.5 T are currently available, but further advances should occur shortly.

We wish to thank Dr. Fang Shu for making the myoglobin expression system available to us and Dr. Melanie Cocco for advice on sample preparation. We also wish to thank Dr. Dan Garrett for providing data analysis software. This research was supported by Grant GM33225 from the National Institutes of Health and benefitted from instrumentation provided by National Science Foundation Grant NSF CHE9413445.

1. Edison, A. S., Abildgaard, F., Westler, W. M., Mooberry, E. S. & Markley, J. L. (1994) *Methods Enzymol.* **239,** 3–79.
2. Wüthrich, K. (1994) *Curr. Opin. Struct. Biol.* **4,** 93–99.
3. Oldfield, E. & Rothgeb, T. M. (1980) *J. Am. Chem. Soc.* **102,** 3635–3637.
4. Bastiaan, E. W., Maclean, C., Van Zijl, P. C. M. & Bothner-By, A. A. (1987) *Annu. Rep. NMR Spectrosc.* **19,** 35–77.
5. Abragam, A. (1961) in *Principles of Nuclear Magnetism* (Clarendon, Oxford), pp. 103–106.
6. Lohman, J. A. B. & Maclean, C. (1979) *Mol. Phys.* **38,** 1255–1261.
7. Horrocks, W. D. W., Jr., & Greenberg, E. S. (1973) *Biochim. Biophys. Acta* **322,** 38–44.
8. Emerson, S. D. & La Mar, G. N. (1990) *Biochemistry* **29,** 1556–1566.
9. Lecomte, J. T. J., Johnson, R. D. & La Mar, G. N. (1985) *Biochim. Biophys. Acta* **829,** 268–274.
10. Emerson, S. D. & La Mar, G. N. (1990) *Biochemistry* **29,** 1545–1556.
11. Banci, L., Bertini, I. & Luchinat, C. (1994) *Methods Enzymol.* **239,** 485–514.
12. Thériault, Y., Pochapsky, T. C., Dalvit, C., Chiu, M. L., Sligar, S. G. & Wright, P. E. (1994) *J. Biomol. NMR* **4,** 491–504.
13. Neidhart, F. C., Bloch, P. L. & Smith, D. F. (1974) *J. Bacteriol.* **119,** 736–747.
14. Shu, F., Ramakrishana, V. & Schoenborn, B. P. (1995) in *Neutrons in Biology*, eds. Knott, R. & Schoenborn, B. P. (Academic, New York), in press.
15. Grzesiek, S. & Bax, A. (1993) *J. Am. Chem. Soc.* **115,** 12593–12594.
16. Kay, L. E., Xu, G. Y. & Yamazaki, T. (1994) *J. Magn. Reson. Ser. A* **109,** 129–133.
17. Wüthrich, K., Wider, G., Wagner, G. & Braun, W. (1982) *J. Mol. Biol.* **155,** 311–318.
18. Cheng, X. & Schoenborn, B. P. (1991) *J. Mol. Biol.* **220,** 381–399.